J. Fluid Mech. (2006), *vol.* 559, *pp.* 205–213.
doi:10.1017/S0022112006000607 Printed in the United Kingdom

Linear energy amplification in turbulent channels

By JUAN C. DEL ÁLAMO[1]† AND JAVIER JIMÉNEZ[1,2]

[1]School of Aeronautics, Universidad Politécnica de Madrid, 28040 Madrid, Spain

[2]Center for Turbulence Research, Stanford University, Stanford, CA 94305, USA

(Received 7 February 2006 and in revised form 26 April 2006)

We study the temporal stability of the Orr–Sommerfeld and Squire equations in channels with turbulent mean velocity profiles and turbulent eddy viscosities. Friction Reynolds numbers up to $Re_\tau = 2 \times 10^4$ are considered. All the eigensolutions of the problem are damped, but initial perturbations with wavelengths $\lambda_x > \lambda_z$ can grow temporarily before decaying. The most amplified solutions reproduce the organization of turbulent structures in actual channels, including their self-similar spreading in the logarithmic region. The typical widths of the near-wall streaks and of the large-scale structures of the outer layer, $\lambda_z^+ = 100$ and $\lambda_z/h = 3$, are predicted well. The dynamics of the most amplified solutions is roughly the same regardless of the wavelength of the perturbations and of the Reynolds number. They start with a wall-normal v event which does not grow but which forces streamwise velocity fluctuations by stirring the mean shear ($uv < 0$). The resulting u fluctuations grow significantly and last longer than the v ones, and contain nearly all the kinetic energy at the instant of maximum amplification.

1. Introduction

The structure of turbulent shear flow has been studied with the aid of linear stability theory for many years. Malkus (1956) obtained a rough approximation to the mean profile of turbulent channel flow by assuming that it should be marginally stable to linear Orr–Sommerfeld perturbation modes. There have been several later attempts, discussed below, to model turbulent structures as unstable or slightly damped modes of the laminar profile. Reynolds & Hussain (1972) studied the stability of the mean turbulent profile, but noted that the right model might have to include an eddy viscosity instead of the molecular one, since the large scales 'feel' the dissipation from the smaller ones. They showed that this approximation reproduces better the behaviour of artificially induced waves in the flow, but they also found that the mean profile is stable at friction Reynolds numbers of the order of one thousand. This discouraged further research on the subject, although Jiménez *et al.* (2001) used the eddy viscosity model to explain the turbulent structures observed in a channel with porous walls, where the mean profile is unstable.

In the meantime it was recognized that even stable three-dimensional disturbances in laminar Poiseuille flow can undergo substantial transient amplification before decaying (Gustavsson 1991; Butler & Farrell 1992; Reddy & Henningson 1993). This behaviour was linked by Butler & Farrell (1992) to the non-orthogonality of

† Present address: Department of Mechanical and Aerospace Engineering, UCSD, La Jolla, CA 92093, USA.

the eigenfunctions of the Orr–Sommerfeld–Squire system, so that different decaying modes can interact constructively to yield transient growth.

In this paper we revisit the stability of the mean velocity profile of a turbulent channel flow, using an eddy viscosity approximation, and relate the modes with the largest transient growth to the large structures observed in real flows. The analysis is presented in § 2, the results are discussed in § 3, and § 4 concludes.

2. The linear model

We consider turbulent channels of height $2h$, with the mean stream aligned along the x-direction and their walls perpendicular to the y-direction. These flows are characterized by their friction Reynolds number, $Re_\tau = u_\tau h/\nu$, where ν is the molecular viscosity and u_τ is the friction velocity. Variables scaled in wall units with ν and u_τ are represented with a $+$ superscript.

The linearized dynamics of small-amplitude perturbations to the mean profile $U(y)$ in a turbulent channel are governed by

$$\partial_t \boldsymbol{u} + U(y)\partial_x \boldsymbol{u} + (v\partial_y U, 0, 0) = -\boldsymbol{\nabla} p + [\nu_T(\partial_{xx} + \partial_{zz}) + \partial_y(\nu_T \partial_y)]\boldsymbol{u}, \tag{2.1}$$

where $\boldsymbol{u} = (u, v, w)$ is the velocity vector of the perturbations, and p is their pressure. This equation differs from the linearized Navier–Stokes equation in the viscous terms, where the constant molecular viscosity is substituted by a variable turbulent eddy viscosity $\nu_T(y)$ to model the interaction of the perturbations with the background turbulence.

Following Reynolds & Hussain (1972), we have used the Cess (1958) analytic approximation for the turbulent eddy viscosity,

$$\nu_T = \frac{\nu}{2}\left\{1 + \frac{K^2 Re_\tau}{9}[2\eta - \eta^2][3 - 4\eta + \eta^2]^2\left[1 - \exp\left(\frac{-\eta Re_\tau}{A}\right)\right]^2\right\}^{1/2} + 1/2, \tag{2.2}$$

where $\eta = y/h$ and the molecular viscosity ν is also included. The mean velocity profile is given by integrating $(1-\eta)u_\tau^2/\nu_T(\eta)$. Apart from the Reynolds number, the Cess formula has two parameters that we have fixed by least-square fitting the mean profile from the numerical channel results of Hoyas & Jiménez (2006) at $Re_\tau = 2000$. The resulting values of the parameters, $A = 25.4$ and $K = 0.426$, compare reasonably well with the ones used by Reynolds & Hussain (1972), $A = 29$ and $K = 0.45$, and have been kept constant for all the Reynolds numbers explored in this work. The profile from Hoyas & Jiménez (2006) is shown in figure 1(*a*), together with the ones obtained with (2.2) for $A = 25.4$ and $K = 0.426$ at different Reynolds numbers. The analytic profiles agree with the experimental one and follow the classical logarithmic law with $\kappa = 0.41$ and $B = 5.2$. The corresponding eddy viscosities are represented in figure 1(*b*). They scale in wall units near the wall and follow the similarity law $\nu_T = u_\tau \kappa y$ in the logarithmic layer. In the outer region, both the velocity defect $U(h) - U(y)$ and the eddy viscosities scale with h and u_τ (not shown).

Combining (2.1) with the continuity equation the pressure term can be eliminated to obtain modified Orr–Sommerfeld and Squire equations for v and for the wall-normal vorticity, ω_y. If we assume wave-like perturbations, $\boldsymbol{q} = [\widehat{v}(y), \widehat{\omega}_y(y)] \times \exp[\mathrm{i}(k_x x + k_z z - \sigma t)]$, these equations are

$$\{(k_x U - \sigma)\nabla^2 - k_x \partial_{yy} U + \mathrm{i}\nabla^2[\partial_y(\nu_T \partial_y) - k^2 \nu_T]\}\widehat{v} = 0, \tag{2.3}$$

$$\{(k_x U - \sigma) + \mathrm{i}[\partial_y(\nu_T \partial_y) - k^2 \nu_T]\}\widehat{\omega}_y = -k_z \widehat{v}\partial_y U, \tag{2.4}$$

with boundary conditions $\widehat{v} = \partial_y \widehat{v} = \widehat{\omega}_y = 0$ at the walls. The streamwise and spanwise wavenumbers are k_x and k_z, and $k^2 = k_x^2 + k_z^2$. The complex eigenfunctions of the

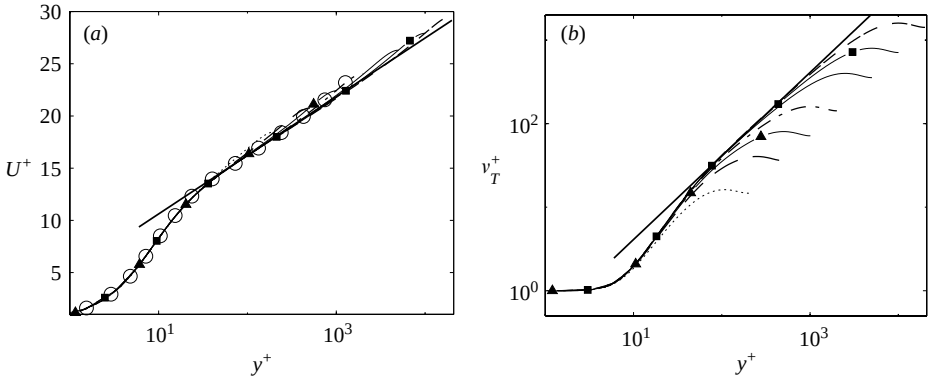

FIGURE 1. (*a*) Cess (1958) mean profiles at different Reynolds numbers; ○, direct simulation of a $Re_\tau = 2000$ channel (Hoyas & Jiménez 2006); the solid straight line is $U^+ = 1/\kappa \log y^+ + B$ with $\kappa = 0.41$ and $B = 5.2$. (*b*) Cess eddy viscosities; the solid straight line is $v_T^+ = \kappa y^+$. ·····, $Re_\tau = 200$; — — —, $Re_\tau = 500$; — ▲ —, $Re_\tau = 10^3$; — · —, $Re_\tau = 2 \times 10^3$; ———, $Re_\tau = 5 \times 10^3$; — ■ —, $Re_\tau = 10^4$; -- --, $Re_\tau = 2 \times 10^4$.

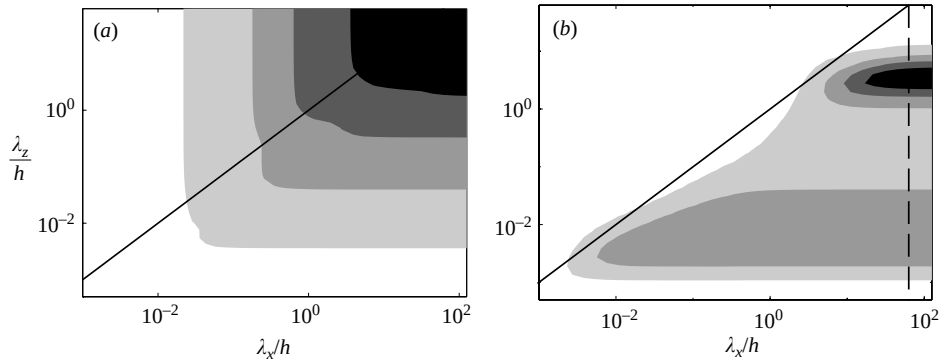

FIGURE 2. (*a*) Imaginary part $\sigma_{I,1} h/u_\tau$ of the least damped eigenvalue of (2.3)–(2.4), represented as a function of λ_x/h and λ_z/h. The levels represented are, from dark to light, $-1(\times 10) - 1000$. (*b*) Maximum transient growth G as a function of λ_x/h and of λ_z/h. The levels represented are, from light to dark, 1.5(+1)4.5. The solid straight line is $\lambda_x = \lambda_z$. The dashed vertical line is $\lambda_x = 60h$. In both figures $Re_\tau = 2 \times 10^4$.

problem are $\widehat{v}(y)$ and $\widehat{\omega}_y(y)$, and their associated eigenvalue is $\sigma = \sigma_R + \mathrm{i}\sigma_I$. The real part σ_R/k_x is the advection velocity of the perturbation, and the imaginary part, σ_I, determines the temporal stability. The problem is unstable if $\sigma_I > 0$ for at least one eigensolution.

We have discretized (2.3) and (2.4) using a Chebyshev spectral collocation method. The resulting eigenvalue problem has been solved numerically, varying simultaneously k_x, k_z and Re_τ. We will present results for $Re_\tau = 2 \times 10^2$–2×10^4, using numerical resolutions from $N_y = 130$ to $N_y = 514$ grid points, which are enough to resolve the eigenfunctions for the smallest waves considered at each Reynolds number.

3. Results and discussion

Figure 2(*a*) extends the results of Reynolds & Hussain (1972) to $Re_\tau = 2 \times 10^4$. It shows that the imaginary part $\sigma_{I,1}$ of the least damped eigenvalue of (2.3)–(2.4)

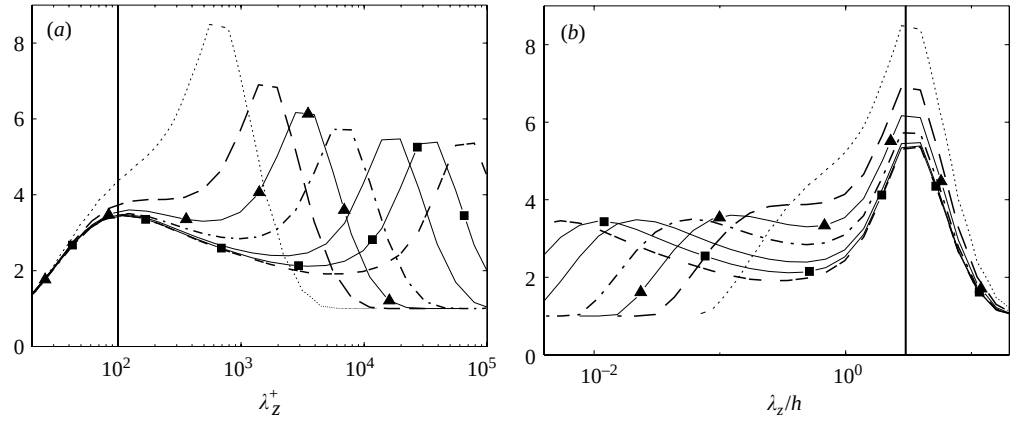

FIGURE 3. Maximum energy amplification $G(60h, \lambda_z)$ for fixed disturbance length and different Reynolds numbers. Lines and symbols as in figure 1. (*a*) $G(60h, \lambda_z^+)$; the solid vertical line is $\lambda_z^+ = 100$. (*b*) $G(60h, \lambda_z/h)$; the solid vertical line is $\lambda_z = 3h$.

is negative for all combinations of the perturbation wavelengths $\lambda_x = 2\pi/k_x$ and λ_z, implying that any disturbance decays after enough time.

Nevertheless, some particular disturbances grow before decaying, due to the non-normality of the eigenfunctions. Figure 2(*b*) displays the maximum energy amplification

$$G(\lambda_x, \lambda_z) = \max_{\boldsymbol{q}(t=0)\neq\boldsymbol{0}} \left[\frac{\|\boldsymbol{q}(\lambda_x, \lambda_z, t)\|}{\|\boldsymbol{q}(\lambda_x, \lambda_z, t=0)\|} \right], \tag{3.1}$$

where $\|\boldsymbol{q}(\lambda_x, \lambda_z, t)\|$ is the kinetic energy contained in the perturbation with wavelengths λ_x and λ_z at time t. The maximum amplification is computed by applying to (2.3)–(2.4) the procedures detailed in Reddy & Henningson (1993). The method also produces the most amplified solutions and the optimal initial conditions. Figure 2(*b*) indicates that there is transient energy growth for $\lambda_x \gtrsim \lambda_z$, consistent with the streamwise-elongated structures commonly observed in turbulent channels. For each value of λ_z, the maximum energy amplification initially grows with the streamwise wavelength but becomes constant for very long perturbations. For simplicity, we will focus on this range of asymptotic λ_x independence.

The maximum amplification is locally highest in two parts of the wavelength plane, one at small scales and the other at very large ones. Since turbulence acts as a continuous source of random disturbances of all sizes, the regions of high amplification in figure 2(*b*) should be associated with prevalent structures in the flow. This is explored in figures 3(*a*) and 3(*b*) by displaying G as a function of λ_z for different Reynolds numbers. In all cases $\lambda_x = 60h$, which is represented by the dashed line in figure 2(*b*).

Figure 3(*a*) shows that expressing the widths in wall units collapses the positions of the small-scale peaks of G around $\lambda_z^+ = 100$. This agrees remarkably well with the width of the near-wall streaks (Smith & Metzler 1983), and suggests that the genesis of those structures is captured at least approximately by our linear model. The same is true for the large global structures documented by del Álamo & Jiménez (2003) and del Álamo *et al.* (2004). They have widths of the order of $\lambda_z = 3h$, similar to the common position of the large-scale peaks of G in figure 3(*b*). Notice that due to the independence of G from λ_x for long modes (see figure 2*b*), these results are

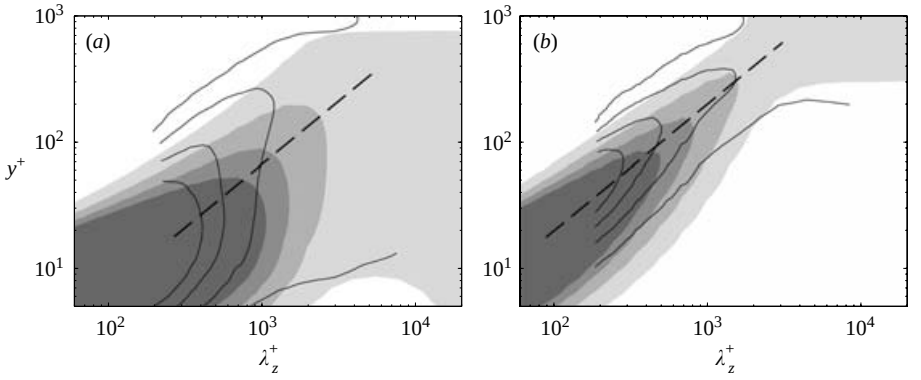

FIGURE 4. Amplitudes of u and v taken at $\lambda_x = 15h$ and represented as functions of λ_z and y. The shaded contours come from (2.3)–(2.4) at $Re_\tau = 10^3$. The line contours come from the principal POD eigenfunction from the $Re_\tau = 950$ channel flow of del Álamo *et al.* (2004). Both sets of data have been normalized for each λ_z to yield unit integrated energy across the channel height. The levels represented are 0.5(+0.5)2.0. (*a*) u; the model data come from the most amplified solution; ———, $\lambda_z = 15y$. (*b*) v; the model data come from the optimal initial condition; ———, $\lambda_z = 5y$.

representative for the observed lengths of the near-wall streaks ($\lambda_x^+ \approx 1000$, Jiménez, del Álamo & Flores 2004) and of the global structures ($\lambda_x \approx 10h$, del Álamo & Jiménez 2003).

The presence of two local maxima in $G(\lambda_x, \lambda_z)$ contrasts with the single maximum found by Reddy & Henningson (1993) for the laminar case, which is located at $\lambda_z \approx 3.1h$ at different Reynolds numbers, in agreement with the position of the wide-λ_z maximum in figure 3(*b*). Butler & Farrell (1993) obtained maximum growth for $\lambda_z \approx 3.0h$ using a turbulent profile and a constant molecular viscosity at $Re_\tau = 180$. These authors were however only able to obtain an optimal solution with $\lambda_z^+ = 100$ at the same Reynolds number by constraining the maximum growth time. In the present case the $\lambda_z^+ = 100$ peak of G appears naturally at different Reynolds numbers as a consequence of the scale separation induced by the variable eddy viscosity. This idea has been checked by solving (2.3)–(2.4) at $Re_\tau = 5 \times 10^3$ with a constant eddy viscosity equal to the average along y of that given in (2.2). In that case the maximum transient growth only has one narrow peak at $\lambda_z = 3h$. Figure 3(*b*) also suggests that the Reynolds number used by Butler & Farrell (1993) might have been too low to distinguish between the two peaks.

The relation between the present results and the turbulent structures in real channels is further tested in figures 4(*a*) and 4(*b*). The shaded contours in those figures are isolines of the maximum $|u|$ and $|v|$ in the optimal solutions, represented as functions of the perturbation width and of the wall distance, and taken at $\lambda_x = 15h$ and $Re_\tau = 1000$. We have represented u at the instant of maximum amplification, and v at $t = 0$ because, as we will see below, those are the times when each velocity component is most intense in the present model. The line contours represent the amplitudes of u and v in the most energetic eigenfunctions of the proper orthogonal decomposition (POD) of the velocity field from the $Re_\tau = 950$ channel flow of del Álamo *et al.* (2004), computed at roughly the same fixed λ_x as the model. The POD eigenfunctions have been computed from the two-point spectral density tensor of the velocity vector as described by Moin & Moser (1989). Note that data at the previously used $\lambda_x = 60h$ are not available from the direct simulations.

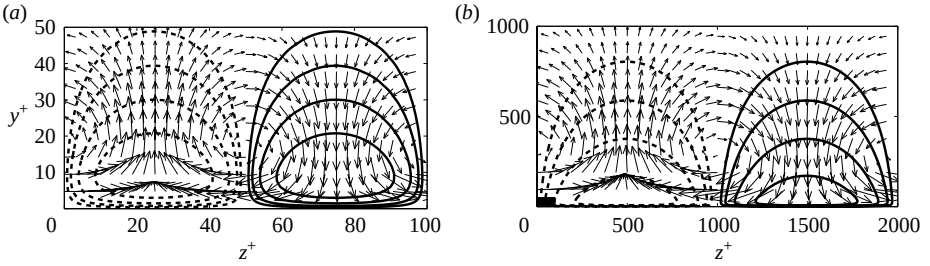

FIGURE 5. Transverse view of the optimal solution for $\lambda_x = 60h$, $Re_\tau = 2 \times 10^4$. The arrows indicate the initial (v, w) field and the longest one is unity in the same arbitrary units used for u. The contours represent the most amplified streamwise velocity and the levels represented are $0.125(\times 2)2$. The solid contours are $u > 0$ and the dashed ones are $u < 0$. (*a*) $\lambda_z^+ = 100$. (*b*) $\lambda_z^+ = 2000$; the small solid black box in the bottom left corner is the size of the axes in (*a*).

The agreement between the linear model and the POD data is good for both velocity components, especially taking into account that the parameters of the model have been chosen to fit only the experimental mean profile. The intensity of $|u|$ peaks around $y^+ \approx 10$ for $\lambda_z^+ = 100$, which agrees well with the properties of the sublayer streaks, and the wide-λ_z part of the optimal solution, that was identified above with the global modes, in fact spans the whole channel height.

It is interesting that the present model is able to reproduce the self-similar spreading of the velocity structures in the overlap region, which has been represented in figures 4(*a*) and 4(*b*) by the dashed lines $\lambda_z \sim y$, and which has been documented by Nakagawa & Nezu (1981), del Álamo & Jiménez (2003) and Tomkins & Adrian (2003).

Figures 5(*a*) and 5(*b*) are representations in $z - y$ physical space of two most amplified single-wave solutions at $Re_\tau = 2 \times 10^4$ and $\lambda_x = 60h$. The first one has $\lambda_z^+ = 100$, and the second one $\lambda_z^+ = 2000$. Both contain streamwise velocity streaks of alternating signs flanked by a pair of counter-rotating streamwise vortices. This is similar to the widely documented statistical organization of the buffer layer (for a review, see Robinson 1991), but notice that the structures in figure 5(*b*) are much larger than the buffer layer streaks in figure 5(*a*), and that they reach deep into the logarithmic layer. This is emphasized in figure 5(*b*) by representing as a black box the axes of figure 5(*a*). These logarithmic layer structures agree with the growing evidence that the flow above the buffer layer contains long regions of high or low u, both in channels (Jiménez 1998) and in boundary layers (Hutchins, Ganapathisubramani & Marusic 2004). More recently, del Álamo *et al.* (2006) showed that, when those structures are identified by using the average velocity field conditioned with the presence of vortex clusters in the logarithmic region, they appear as conical u streaks surrounded by pairs of counter-rotating streamwise vortices.

The dynamics of the present optimal solutions are analysed in figures 6(*a*) and 6(*b*). This analysis is motivated by the agreement shown above between the optimal solutions and the experimental data, and is carried out with the aim of shedding some light on the behaviour of the solutions to the full nonlinear equations, which are much harder to study. Figure 6(*a*) shows the streamwise and transverse components of the energy growth, $G_u = u^2(t)/[2\|q(0)\|]$ and $G_{v,w} = [v^2(t) + w^2(t)]/[2\|q(0)\|]$. The data are presented for $\lambda_x = 60h$ and $Re_\tau = 2 \times 10^4$, and are given as functions of λ_z and of time. The latter is normalized with the instant of maximum energy amplification, t_M, which is a function of λ_z. Initially, almost all the kinetic energy is contained in the

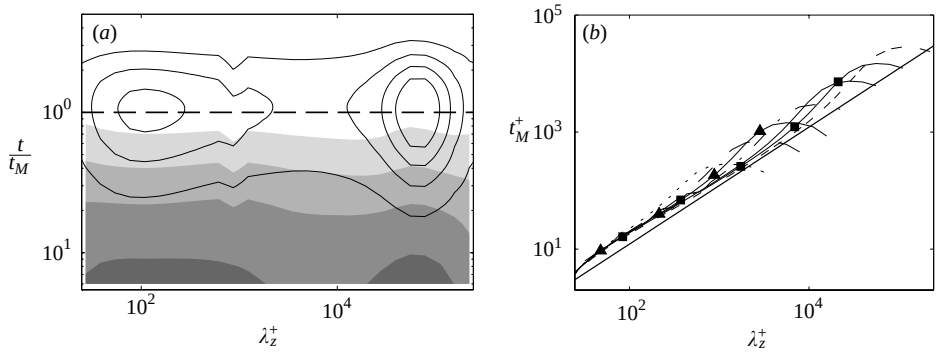

FIGURE 6. (*a*) Component-wise energy amplification as a function of λ_z^+ and of t/t_M; $\lambda_x = 60h$; $Re_\tau = 2 \times 10^4$; the line contours come from the streamwise component, G_u, and the levels represented are 1(+1)4; the shaded contours come from the transverse component, $G_{v,w}$, and the levels represented are 0.2(+0.2)0.8. (*b*) Time t_M^+ of maximum amplification as a function of λ_z^+; $\lambda_x = 60h$; lines and symbols as in figure 1; the solid straight line is $t_M^+ = \lambda_z^+/10$.

transverse motions that decay with time under the effect of the eddy viscosity. While decaying, these motions generate streamwise velocity fluctuations through the $k_z \widehat{v} \partial_y U$ Squire's forcing term, consistent with the negative value of uv inside the streaks in figures 5(*a*) and 5(*b*). At $t \approx t_M$, immediately after the v forcing has decayed, G_u reaches its maximum. Its value is approximately equal to the highest values of G in figure 2(*b*), indicating that the energy growth in the present model occurs mainly in the streamwise component.

The implication is that the development of the u fluctuations is passive, in the sense that it is produced by the stirring of the mean profile caused by previously existing transverse motions. This result is consistent with the autonomous wall experiments of Jiménez *et al.* (2004), who damped artificially the wall-normal velocity in a band of wavelengths and observed a proportional decrease of u in the same band. However, the present model does not offer a direct answer for the origin of the v structures that trigger transient growth. This is common to other linear models. Jovanović & Bamieh (2004) performed an input–output analysis of the perturbation equations for the laminar case, and showed that transverse velocity perturbations led to strong amplifications of u, while streamwise velocity perturbations produced little effect on v and w. There are numerous works on the stability of the sublayer streaks (see for instance Schoppa & Hussain 2002) showing that they must have a finite amplitude before they become unstable. Such effects are absent from any linear model, but the present results provide a mechanism by which the streaks, both in the sublayer and above it, can become strong enough to be unstable. Schoppa & Hussain (2002) show that transient growth of damped eigenfunctions of finite-amplitude sublayer streaks is the most likely mechanism for the formation of new quasi-streamwise vortices.

Notice that the dynamics of the present optimal solutions depend little on their size when time is normalized with t_M, as in figure 6(*a*). That is interesting because t_M depends linearly on λ_z (figure 6*b*), and therefore the evolution of any perturbation that is initially spatially compact is self-similar in our model. Such initial conditions have roughly white spectra both in the wave space and in the space of the eigenfunctions of (2.3)–(2.4), and develop according to the most amplified solution for each wavelength. This will occur at the corresponding time scale t_M of each wave mode, so that the size

of the perturbation in physical space will increase linearly with time. In agreement with this, del Álamo *et al.* (2006) showed that the lifetimes of the v structures in the logarithmic region of turbulent channels are proportional to their sizes.

Figure 6(b) also offers an explanation for the Reynolds-number scaling of the intensities of the peaks of G in figures 3(a) and 3(b). Apart from a small decrease at low Reynolds numbers, these intensities are independent of Re_τ, which contrasts with the laminar case, where the maximum energy amplification grows as Re^2 (Gustavsson 1991; Butler & Farrell 1992; Reddy & Henningson 1993). This difference can be reconciled if the effective Reynolds number of the most amplified solutions remains roughly constant. In fact, if we define the effective Reynolds number as $Re_T = \lambda_z^2/(t_M \nu_T)$ and assume that $\nu_T = u_\tau \lambda_z$ in the logarithmic region, the solid line straight line in figure 6(b) represents $Re_T = 10$. The resulting low value of the effective Reynolds number would also explain the relatively moderate values of the maximum amplification obtained with the turbulent viscosity. In the laminar case, there is no energy growth for $Re = 10$ and the maximum energy growth for $Re = 100$ is $G_{max} \approx 2.3$.

4. Conclusions

We have shown that the dominant structures of the streamwise velocity in turbulent channels are described well by the linear modes with the largest transient growth from the Orr–Sommerfeld–Squire equations for the mean turbulent profile, computed using the eddy viscosity required to maintain that profile. Two maxima are found. One corresponds to the sublayer streaks and the other one to the large-scale global structures spanning the full channel. These two peaks separate well when the Reynolds number is large enough, and scale respectively in inner and outer units. The intermediate minimum is not very pronounced, and describes self-similar modes that agree well with the observed structures of the logarithmic layer.

The structures for the transverse velocity also agree well with the highest-growth solutions, although they decay quickly both in the linear model and in direct simulations, and act mainly as 'seeds' for the longer-lived and stronger structures of the streamwise velocity.

This work was supported in part by the Spanish CICYT contract DPI2003-03434. It is a pleasure to acknowledge fruitful discussions with Oscar Flores.

REFERENCES

del Álamo, J. C. & Jiménez, J. 2003 Spectra of the very large anisotropic scales in turbulent channels. *Phys. Fluids* **15**, L41–L44.

del Álamo, J. C., Jiménez, J., Zandonade, P. & Moser, R. D. 2004 Scaling of the energy spectra of turbulent channels. *J. Fluid Mech.* **500**, 135–144.

del Álamo, J. C., Jiménez, J., Zandonade, P. & Moser, R. D. 2006 Self-similar vortex clusters in the turbulent logarithmic region. *J. Fluid Mech.* (in press).

Butler, K. M. & Farrell, B. F. 1992 Three-dimensional optimal perturbations in viscous shear flow. *Phys. Fluids* A **4**, 1637–1650.

Butler, K. M. & Farrell, B. F. 1993 Optimal perturbations and streak spacing in wall-bounded shear flow. *Phys. Fluids* A **5**, 774–777.

Cess, R. D. 1958 A survey of the literature on heat transfer in turbulent tube flow. *Rep.* 8-0529-R24. Westinghouse Research.

Gustavsson, L. H. 1991 Energy growth of three-dimensional disturbances in plane poiseuille flow. *J. Fluid Mech.* **224**, 241–260.

Hoyas, S. & Jiménez, J. 2006 Scaling of the velocity fluctuations in turbulent channels up to $Re_\tau = 2003$. *Phys. Fluids* **18**, 011702.

Hutchins, N., Ganapathisubramani, B. & Marusic, I. 2004 Dominant spanwise Fourier modes, and the existence of very large coherence in turbulent boundary layers. In *15th Australasian Fluid Mechanics Conference* (ed. M. Behnia, W. Lin & G. D. McBain). AMC00127.

Jiménez, J. 1998 The largest structures in turbulent wall flows. In *Annu. Res. Briefs*, pp. 943–945. Center for Turbulence Research, Stanford University.

Jiménez, J., del Álamo, J. C. & Flores, O. 2004 The large-scale dynamics of near-wall turbulence. *J. Fluid Mech.* **505**, 179–199.

Jiménez, J., Uhlmann, M., Pinelli, A. & Kawahara, G. 2001 Turbulent shear flow over active and passive porous surfaces. *J. Fluid Mech.* **442**, 89–117.

Jovanović, M. R. & Bamieh, B. 2004 Componentwise amplification in channel flows. *J. Fluid Mech.* **534**, 145–183.

Malkus, W. V. R. 1956 Outline of a theory of turbulent shear flow. *J. Fluid Mech.* **1**, 521–539.

Moin, P. & Moser, R. D. 1989 Characteristic-eddy decomposition of turbulence in a channel. *J. Fluid Mech.* **200**, 471–510.

Nakagawa, H. & Nezu, I. 1981 Structure of space-time correlations of bursting phenomena in an open channel flow. *J. Fluid Mech.* **104**, 1–43.

Reddy, S. C. & Henningson, D. S. 1993 Energy growth in viscous channel flows. *J. Fluid Mech.* **252**, 209–238.

Reynolds, W. C. & Hussain, A. K. M. F. 1972 The mechanics of an organized wave in turbulent shear flow. Part 3. Theoretical models and comparisons with experiments. *J. Fluid Mech.* **54**, 263–288.

Robinson, S. K. 1991 Coherent motions in the turbulent boundary layer. *Annu. Rev. Fluid Mech.* **23**, 601–639.

Schoppa, W. & Hussain, F. 2002 Coherent structure generation in near-wall turbulence. *J. Fluid Mech.* **453**, 57–108.

Smith, C. R. & Metzler, S. P. 1983 The characteristics of low-speed streaks in the near-wall region of a turbulent boundary layer. *J. Fluid Mech.* **129**, 27–54.

Tomkins, C. D. & Adrian, R. J. 2003 Spanwise structure and scale growth in turbulent boundary layers. *J. Fluid Mech.* **490**, 37–74.